# NEW DEVELOPMENT OF TWO-STEP PROCESSING APPROACH FOR SPOTLIGHT SAR FOCUSING IN PRESENCE OF SQUINT

**Ya-Jun Mo[1, 2, \*], Yun-Kai Deng[1], Yun-Hua Luo[1, 2], Bing-Ji Zhao[1, 2], and He Yan[1, 2]**

[1]Institute of Electronics, Chinese Academy of Sciences (IECAS), Beijing 100190, China

[2]Graduate University, Chinese Academy of Sciences (GUCAS), Beijing 100039, China

**Abstract**—This paper analyzes the azimuth spectrum folding problem which arises from the dependence of the Doppler centroid on range frequency in squinted spotlight synthetic aperture radar (SAR). Based on the analysis, a novel approach for squinted spotlight SAR is proposed in this paper. In this approach, an azimuth preprocessing step including a deramping operation and an operation of azimuth spectrum replicating and filtering is introduced to eliminate spectrum folding problem. Then, a modified Range Migration Algorithm (RMA) is adopted to process the preprocessed data. This approach extends the focusing capacity of traditional two-step processing approach from broadside spotlight SAR to squinted case. Moreover, this approach is efficient due to a limited azimuth data extension to resolve the spectrum aliasing problem. Experimental results on simulated raw data validate the proposed approach.

## 1. INTRODUCTION

Synthetic aperture radar (SAR) is an active imaging sensor which can work in any weather condition during the day and night [1, 2]. SAR can be operated in different imaging modes. The standard mode called stripmap mode is widely employed when the antenna pointing direction is held constant as the SAR platform moves on. In spotlight mode [3, 4], azimuth beam illuminates always the same area of the ground

by steering the radar antenna to a fixed point on the ground during the overall illumination time. Consequently, the illumination time of targets is augmented, and a finer azimuth resolution can be achieved. Benefited from the increased illumination time, spotlight SAR can provide more detailed contents for targets detection, identification and classification. Most recently, some advanced SAR systems with spotlight mode can get the best resolution of 0.1m for airborne SAR and 1m for spaceborne SAR [5, 6].

Azimuth beam steering in spotlight mode leads to greater azimuth bandwidth besides finer azimuth resolution. However, to relieve the range ambiguity problem and the burden of large amount of data, the pulse repetition frequency (PRF) is generally smaller than the azimuth bandwidth in spaceborne spotlight SAR or super-resolution airborne spotlight SAR systems [7–9]. As a result, the azimuth spectrum folding phenomenon occurs. This limits the application of frequency domain imaging algorithms for stripmap mode to process spotlight data directly. One solution to overcome the spectrum folding problem is based on a nontrivial reconstruction of the unfolded azimuth spectrum from the folded one by oversampling [10, 11]. The subaperture technique is a completely different approach [12]. R. Lanari proposed a simpler and more efficient two-step processing approach (TSPA) by applying the SPECtral Analysis (SPECAN) technique [7, 8]. The approach introduces an azimuth deramping step to solve the azimuth spectral folding problem and then employs traditional stripmap mode imaging algorithms to obtain focused images. The key point of this approach is to combine the advantages of the computational efficiency of SPECAN algorithm and the precision of stripmap mode imaging algorithms.

Different from conventional spotlight SAR, the radar antenna beam is aimed with a certain angle off the broadside direction in squinted spotlight SAR, with the potential to provide more information about surface structure [13, 14]. Furthermore, squinted mode can also increase the flexibility, so that a desired area on the earth surface is imaged within a single pass of the platform. In squinted spotlight mode, the aliased azimuth spectrum is not only caused by azimuth beam steering but also by the squint angle [15–17]. Consequently, traditional TSPA fails in the squinted case [16, 17]. In this paper, properties of the azimuth spectrum and the azimuth spectral folding phenomenon in squinted spotlight SAR are analyzed. Based on the analysis results, an operation of azimuth spectrum replicating and filtering is added to the azimuth preprocessing step of traditional TSPA to resolve the azimuth spectrum folding problem. After the azimuth preprocessing step, a modified Range Migration Algorithm (RMA)

with modified Stolt interpolation [18, 19] is performed to obtain precise focused image.

In this paper, properties of the azimuth spectrum and the azimuth spectral folding phenomenon in the squinted spotlight SAR are analyzed. Based on the analysis results, an operation of azimuth spectrum replicating and filtering is added to the azimuth preprocessing step of traditional TSPA to resolve the azimuth spectrum folding problem in the squinted spotlight mode. After the azimuth preprocessing step, a modified Range Migration Algorithm (RMA) with a modified Stolt interpolation [18, 19] is performed to obtain precise focused image.

This paper is arranged as follows. In Section 2, a brief description of the imaging geometry in the squinted spotlight mode is given and the properties of the azimuth spectrum are analyzed. Section 3 focuses on the proposed imaging approach. Simulation results on simulated raw data are given in Section 4 to validate the proposed approach. Finally, conclusions are given in Section 5.

## 2. SQUINTED SPOTLIGHT MODE

### 2.1. Imaging Geometry and Signal Model

The planar imaging geometry of the squinted spotlight mode is shown in Fig. 1. The SAR sensor travels along the azimuth direction. The synthetic aperture center is at point $O$, which is also the azimuth time zero. $(x_c, r_c \cos \theta_0)$ represents the observed scene center, where $\theta_0$ is the
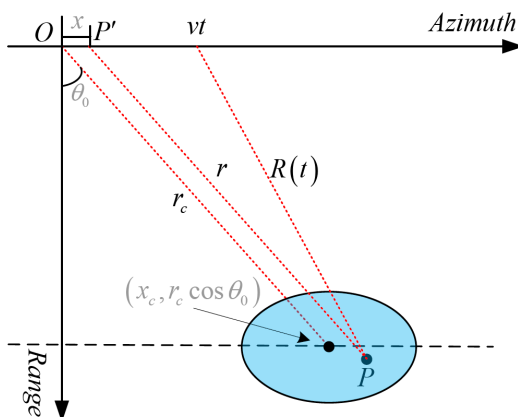


**Figure 1.** Squinted spotlight mode planar imaging geometry.

squint angle, and $r_c$ is the slant range between the synthetic aperture center and the observed scene center. $P$ is a point target at position $(x, r\cos\theta_0)$ in the imaged swath, where $r$ is the slant range from the SAR sensor to the target along the squint direction, i.e., $r = \overline{PP'}$, $x$ is the distance between the synthetic aperture center and point $P'$, $v$ represents the effective radar velocity, and $t$ denotes the azimuth time.

From the imaging geometry in Fig. 1, the expression of instantaneous range $R(t)$ can be obtained as follows:

$$R(t) = \sqrt{r^2 + v^2 (t - t_x)^2 - 2rv(t - t_x)\sin\theta_0}$$

$$\approx r - v\sin\theta_0 (t - t_x) + \frac{v^2\cos^2\theta_0}{2r}(t - t_x)^2 + \cdots \quad (1)$$

with $t_x = x/v$. The echo signal of point target $P$ can be written as (neglecting the constants and inessential amplitude factors):

$$s(\tau, t; x, r) = \mathrm{rect}\left[\frac{\tau - 2R(t)/c}{T_r}\right] \mathrm{rect}\left[\frac{t}{T_{spot}}\right] \exp\left\{-j\frac{4\pi R(t)}{\lambda}\right\}$$

$$\exp\left\{j\pi K_r \left(\tau - 2R(t)/c\right)^2\right\} \quad (2)$$

where $\tau$ is the range time, $T_{spot}$ the full synthetic aperture time, $\lambda = c/f_c$ the center wavelength, and $K_r$ the chirp rate.

## 2.2. Azimuth Spectrum Analysis

Because the analysis is focused on the azimuth signal properties of the squinted spotlight mode, the azimuth signal component is mainly considered in the following [8]. By neglecting the constants and inessential amplitude factors, the simplified expression of azimuth signal component of point target $P$ can be expressed as:

$$s_a(t; x, r) \approx \mathrm{rect}\left[\frac{t}{T_{spot}}\right]\exp\left\{j\frac{4\pi v\sin\theta_0}{\lambda}(t - t_x) - j\pi\frac{2v^2\cos^2\theta_0}{\lambda r}(t - t_x)^2\right\} \quad (3)$$

For simplicity, the high order terms in (3) are neglected without losing the rationale of the discussion [8]. However, the high order terms are still compensated in the following processing steps. Using the Principle of Stationary Phase (POSP), transformation of (3) to the azimuth frequency domain yields

$$S_a\left(f_a;x,r\right)\approx\text{rect}\left[\frac{f_a-f_{dc}-K_at_x}{K_aT_{spot}}\right]\exp\left\{j\pi\frac{f_a^2}{K_a}-j2\pi f_a\frac{f_{dc}}{K_a}-j2\pi f_at_x\right\}$$
$$(4)$$

where $f_a$ is the azimuth frequency, $f_{dc}=\frac{2v\sin\theta_0}{\lambda}$ the Doppler centroid, and $K_a=\frac{2v^2\cos^2\theta_0}{\lambda r}$ the Doppler rate.

From the rect[·] function in equation (4), the total bandwidth of the squinted spotlight SAR can be obtained as below:

$$B_{tot}\approx|K_a|\frac{W_a}{v}+|K_a|\,T_{spot}+\frac{2vB_r}{c}\sin\theta_0$$
$$=\frac{2v\cos^2\theta_0}{\lambda r}W_a+\frac{2v\cos\theta_0}{\lambda}\theta_{az}+\frac{2vB_r}{c}\sin\theta_0=B_{wa}+B_{rot}+B_{sq}\,(5)$$

where $W_a$ is the azimuth extension, $B_r$ the transmitted pulse bandwidth, and $\theta_{az}$ the rotation angle of azimuth beam. Of the three parts, the azimuth extension bandwidth $B_{wa}$ and the target Doppler bandwidth $B_{rot}$ caused by azimuth beam steering are the two components of the total Doppler bandwidth in the broadside spotlight mode. The Doppler bandwidth $B_{sq}$ is caused by the squint angle. Fig. 2(a) shows the slow time/frequency diagram (TFD) of broadside spotlight SAR. Considering $B_{sq}$, the total bandwidth of squinted spotlight SAR is as shown in Fig. 2(b), where $f_\tau$ denotes the range frequency.

Since $T_{spot}$ is much longer in spotlight mode than in stripmap mode, $B_{tot}$ is generally greater than PRF. As a result, the azimuth spectrum is folded. However, the spectral folding problem is much more complicated in squinted case than in broadside case. In the 2-D frequency domain, the Doppler centroid can be determined for each range-frequency component as [15, 17]:

$$f_{dc}\left(f_\tau\right)=\frac{2v\left(f_\tau+f_c\right)\sin\theta_0}{c}+\frac{2vf_c\cos^2\theta_0}{cr}x \qquad (6)$$

It can be seen that the squint angle causes nonzero Doppler centroid and 2-D spectrum skewing. The 2-D spectrum skewing originates in the fact that the Doppler centroid varies with the range frequency $f_\tau$ [1, 15]. Therefore, the Doppler centroid wrapping in the 2-D frequency domain and the change of azimuth sampling frequency in TSPA will lead to the discontinuity of the 2-D spectrum, which not only deteriorates the focused quality but also generates "ghost targets" in the final SAR image [16]. To resolve the problems caused by the squint angle, Lanari et al. propose a Doppler centroid correction

method by multiplying a linear phase term with the azimuth echo signal [8]. But this method cannot completely remove the impact of the squinted Doppler bandwidth $B_{sq}$ [16, 17]. In [16, 17], the author introduces an improved Doppler centroid correction method by multiplying a nonlinear phase term with the azimuth echo signal, which can completely solve the Doppler pectrum folding problem in squinted spotlight SAR. However, this method results in the inequality of the Doppler rate, which will lead to azimuth distortion and need special consideration [17, 20].

## 3. IMAGING ALGORITHM

To unfold the aliased Doppler spectrum in squinted spotlight SAR, an improved azimuth preprocessing step is employed in this paper. In addition, an accurate imaging processor should be adopted because the range migration is generally very large in the squinted spotlight SAR. RMA is a most precise imaging algorithm for SAR processing. However, conventional RMA is not suitable to process squinted SAR data because the skewing of 2-D spectrum after conventional Stolt mapping constrains the range dimension extension in focused image. Consequently, a modified RMA with modified Stolt interpolation is
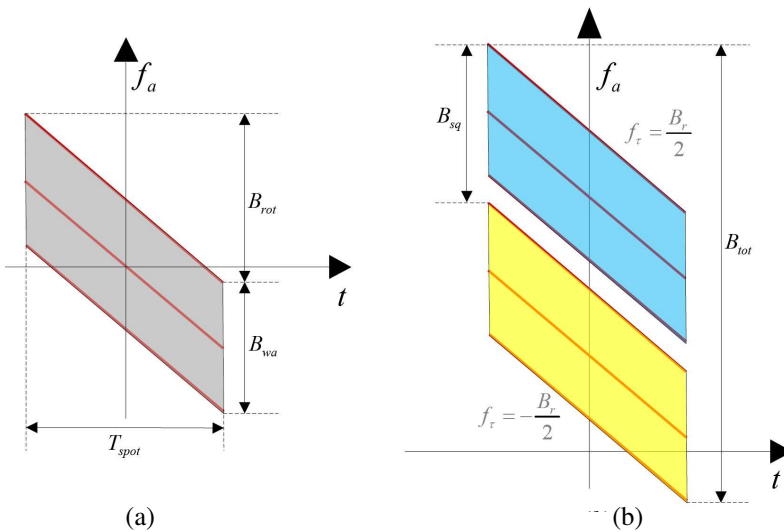


**Figure 2.** (a) The slow time/frequency diagram (TFD) of broadside spotlight mode. (b) The TFD of squinted spotlight mode.

adopted in this paper. The proposed approach includes two important steps: azimuth preprocessing step and precise focusing step. The block diagram is shown in Fig. 3.
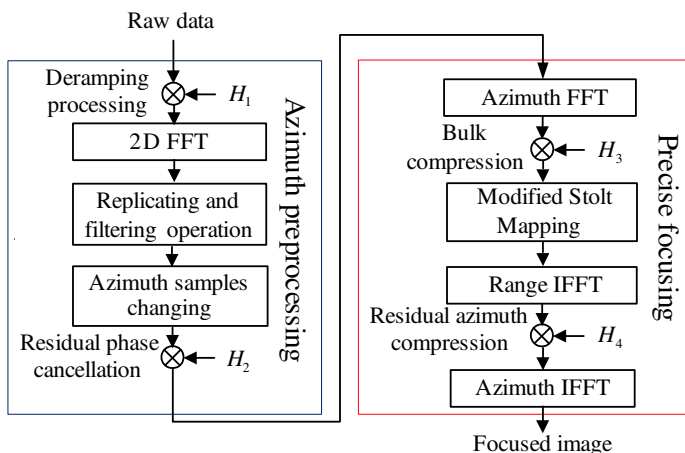


**Figure 3.** Block diagram of the proposed approach.

## 3.1. Azimuth Preprocessing

The azimuth convolution in preprocessing of traditional TSPA essentially involves a deramping-based processing, a subsequent Fourier transform and a residual phase cancelation [16]. The azimuth preprocessing step proposed in this paper, which adds an operation of spectrum replicating and filtering to traditional TSPA, is to resolve the aliased Doppler spectrum due to the squint angle and azimuth beam steering. The spectrum replicating and filtering operation proposed in this paper is carried out before the residual phase cancelation as in Fig. 3. According to traditional TSPA, the selected chirp signal in the azimuth convolution can be written as [8, 16]:

$$g_1(t) = \exp\left\{j\pi K_{a,ref} t^2\right\} \tag{7}$$

where $K_{a,ref} = \frac{2v^2 \cos^2 \theta_0}{\lambda r_{ref}}$ is the azimuth chirp rate and $r_{ref}$ the reference range satisfying $r_{near} \leq r_{ref} \leq r_{far}$. $r_{near}$ and $r_{far}$ represent the nearest and farthest slant ranges of the illuminate spot along the squint direction, respectively. The convolution result between (7) and

(3) can be expressed as:

$$
\begin{aligned}
\tilde{s}_a\left(t;x,r\right) &= \left[s_a\left(t;x,r\right)\exp\left(-j2\pi f_{dc}t\right)\right]\otimes_t g_1\left(t\right) \\
&= \exp\left\{j\pi K_{a,ref}t^2\right\}\int rect\left[\frac{u}{T_{spot}}\right]\exp\left\{-j\pi K_a\left(u-t_x\right)^2\right\} \\
&\quad \exp\left\{j\pi K_{a,ref}u^2\right\}\exp\left\{-j2\pi K_{a,ref}tu\right\}du \qquad (8)
\end{aligned}
$$

where $\otimes_t$ represents the azimuth convolution operator, and $\exp\left(-j2\pi f_{dc}t\right)$ is to remove the Doppler centroid. For the targets located at $r = r_{ref}$, a full azimuth compression effect is obtained. For any other targets with $r \neq r_{ref}$, by using the POSP, the convolution result can be given by:

$$
\tilde{s}_a\left(t;x,r\right) = rect\left[\frac{t-\frac{r_{ref}}{r}t_x}{T_{spot}\left(1-\frac{r_{ref}}{r}\right)}\right]\exp\left\{-j\pi\frac{2v^2\cos^2\theta_0}{\lambda\left(r-r_{ref}\right)}\left(t-t_x\right)^2\right\}
\tag{9}
$$

It can be seen that after azimuth convolution the new Doppler frequency modulation rate becomes:

$$
K'_a = \frac{2v^2\cos^2\theta_0}{\lambda\left(r-r_{ref}\right)}
\tag{10}
$$

Then, the maximum azimuth time extension after the azimuth convolution is given by:

$$
T_{out} = \frac{r_{ref}}{r}\cdot\frac{W_a}{v} + \left|\frac{r-r_{ref}}{r}\right|T_{spot}
\tag{11}
$$

However, because the range extension of the spot area is typically very small, the assumption $|r-r_{ref}| \ll r$ is reasonable [8]. Accordingly, it is easy to obtain $T_{out} < T_{spot}$. Therefore, the azimuth time extension is reduced from $T_{spot}$ to $T_{out}$ after the azimuth convolution. The azimuth convolution eliminates the azimuth spectrum folding problem by increasing the azimuth sampling frequency and compressing the azimuth data extension [8].

Now consider the discrete domain implementation of Equation (8). Assume that $I$ and $\Delta t'$ represent the sampling number and the sampling interval of the azimuth signal, $P_0$ and $\Delta t''$ denote the sampling number and the sampling interval of the output azimuth signal after the azimuth preprocessing step, respectively. Accordingly, by neglecting inessential amplitude factors, Equation (8) can be expressed as:

$$\tilde{s}_a(n \cdot \Delta t''; x, r) = \exp\left\{j\pi K_{a,ref}(n \cdot \Delta t'')^2\right\} \sum_{i=-I/2}^{I/2-1} s_a(i \cdot \Delta t'; x, r)$$

$$\cdot \exp\left\{-j2\pi f_{dc} \cdot i \cdot \Delta t'\right\} \cdot \exp\left\{j\pi K_{a,ref}(i \cdot \Delta t')^2\right\}$$

$$\cdot \exp\left\{-j\pi K_{a,ref}\Delta t' \cdot \Delta t'' \cdot i \cdot n\right\} \tag{12}$$

with $n = -\frac{P_0}{2}, \cdots, \frac{P_0}{2} - 1$. In order to use FFT code, $P_0$ satisfies:

$$K_{a,ref}\Delta t' \cdot \Delta t'' = \frac{2v^2 \cos^2 \theta_0}{\lambda r_{ref}} \Delta t' \cdot \Delta t'' = \frac{1}{P_0} \tag{13}$$

While $\Delta t''$ is selected in agreement with the Nyquist limit:

$$\Delta t'' < 1/B_{tot} \tag{14}$$

Therefore, Equation (12) becomes:

$$\tilde{s}_a(n \cdot \Delta t''; x, r) = \exp\left\{j\pi K_{a,ref}(n \cdot \Delta t'')^2\right\} \cdot DFT\left\{s_a(i \cdot \Delta t'; x, r)\right.$$

$$\cdot \exp\left\{-j2\pi f_{dc} \cdot i \cdot \Delta t'\right\} \cdot \exp\left\{j\pi K_{a,ref}(i \cdot \Delta t')^2\right\}\} \tag{15}$$

According to (15), the selected function $H_1$ in Fig. 3 can be written as:

$$H_1 = \exp\left\{j\pi K_{a,ref}(i \cdot \Delta t')^2 - j2\pi f_{dc} \cdot i \cdot \Delta t'\right\} \tag{16}$$

After multiplying the deramping function (16), the azimuth Doppler centroid becomes:

$$f_{dc}(f_\tau) = \frac{2v f_\tau \sin \theta_0}{c} \tag{17}$$

And the total bandwidth becomes:

$$B'_{tot} = B_{tot} - K_{a,ref}T_{spot} \approx B_{wa} + B_{sq} > PRF \tag{18}$$

Consequently, the azimuth spectrum is still aliased. Fig. 4(a) shows the TFD of multiplying the deramping function (16). The spectrum folding phenomena after deramping is shown in Fig. 4(b). To resolve the residual aliasing problem, an operation of azimuth spectrum replicating and filtering will be introduced in the following. Multiple copies of azimuth data are combined together in the Doppler domain as shown in Fig. 4(c). According to (18), the number of copies can be estimated by:

$$N_f = 2 \left\lceil \frac{B_{wa} + B_{sq}}{2 \cdot PRF} - 0.5 \right\rceil + 1 \tag{19}$$
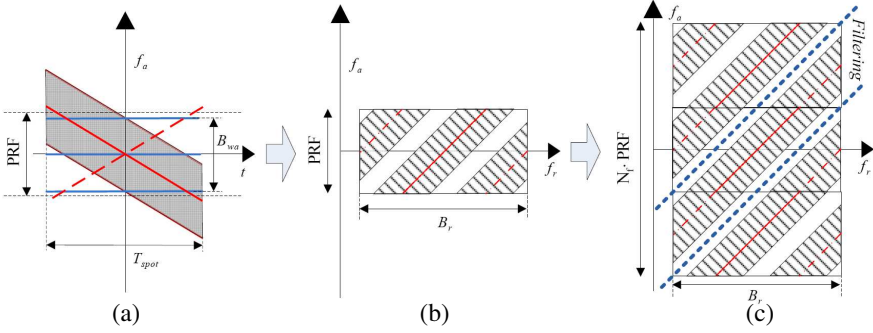
**Figure 4.** (a) The TFD of the deramping operation. (b) Spectrum folding due to the squint angle. (c) Azimuth replicating and filtering operations.

After the azimuth spectrum replicating, a following range frequency variant Doppler filter is adopted to remove the interferential spectrum to obtain the unfolded 2-D spectrum as shown in Fig. 4(c). According to (17), the filter can be given by:

$$H_F(f_r, f_a) = \begin{cases} 1, \text{ with } \left| f_a - \frac{2vf_r}{c} \sin\theta_0 \right| < \frac{\text{PRF}}{2} \\ 0, \text{ otherwise} \end{cases}$$

with

$$f_a \in \left[ -\frac{N_f \cdot \text{PRF}}{2}, \frac{N_f \cdot \text{PRF}}{2} \right]. \tag{20}$$

After the filtering operation, the aliased Doppler spectrum is unfolded. However, the number of azimuth samples increases. In order to keep the efficiency of the proposed algorithm, the new number of the azimuth samples needs to be updated as follows:

$$P_1 = \left\lceil P_0 \cdot \frac{B_{wa} + B_{sq}}{B_{wa}} \right\rceil \tag{21}$$

where $P_0$ denotes the sampling number of the output azimuth signal as mentioned. According to (15), a residual phase cancellation function $H_2$ should be multiplied as shown in Fig. 3:

$$H_2 = \exp\left\{ -j\pi K_{a,ref}(m \cdot \Delta t'')^2 \right\}$$

with

$$m = -\frac{P_1}{2}, \cdots, \frac{P_1}{2} - 1. \tag{22}$$

To compare the performance of traditional TSPA and the proposed approach in this paper, a simulation experiment was carried out. The SAR system parameters are shown in Table 1.

Table 1. System parameters.

| Parameters | Value |
|---|---|
| Carrier frequency | 5.3 GHz |
| Antenna length | 6 m |
| System PRF | 2149 Hz |
| Pulse duration | 1 µs |
| Pulse bandwidth | 100 MHz |
| SAR velocity | 7000 m/s |
| Squint angle | 30° |
| Slant range of imaged center | 300 km |

Figures 5(a)–(c) shows the 2-D spectrum of original signal, the 2-D spectrum processed by traditional TSPA and by the proposed approach in this paper, respectively. It is easy to note that there exists severe azimuth spectrum folding problem in Fig. 5(a). The residual discontinuity distortion still exists in the 2-D spectrum processed by traditional TSPA in Fig. 5(b). In contrast, the unfolded spectrum is well reconstructed in Fig. 5(c).

## 3.2. Precise Focusing Using Modified RMA

After the preprocessing, the azimuth spectrum folding problem is avoided. Therefore, the correlative imaging algorithms for squinted stripmap SAR can be applied to focus the squinted spotlight SAR data. To obtain most precise focused result, a modified RMA [18, 19, 21] with modified Stolt mapping is used in this paper. The first step of the RMA is the reference function multiply (RFM) for bulk focusing which is implemented in the 2-D frequency domain. The transfer function for the RFM can be expressed as:

$$H_3(f_\tau, f_a) = \exp \left\{ j \frac{4\pi r_{ref0}}{c} \sqrt{(f_c + f_\tau)^2 - \frac{c^2 f_a^2}{4v^2}} + j \frac{\pi f_\tau^2}{K_r} \right\} \qquad (23)$$

where $r_{ref0}$ is the reference range. After bulk focusing, targets at the reference range are fully focused, while targets away from the reference range are just partially focused. The residual phase term in the 2-D spectrum is given by:

$$\theta_{RES}(f_\tau, f_a) = -j \frac{4\pi(r - r_{ref0})}{c} \sqrt{(f_c + f_\tau)^2 - \frac{c^2 f_a^2}{4v^2}} \qquad (24)$$
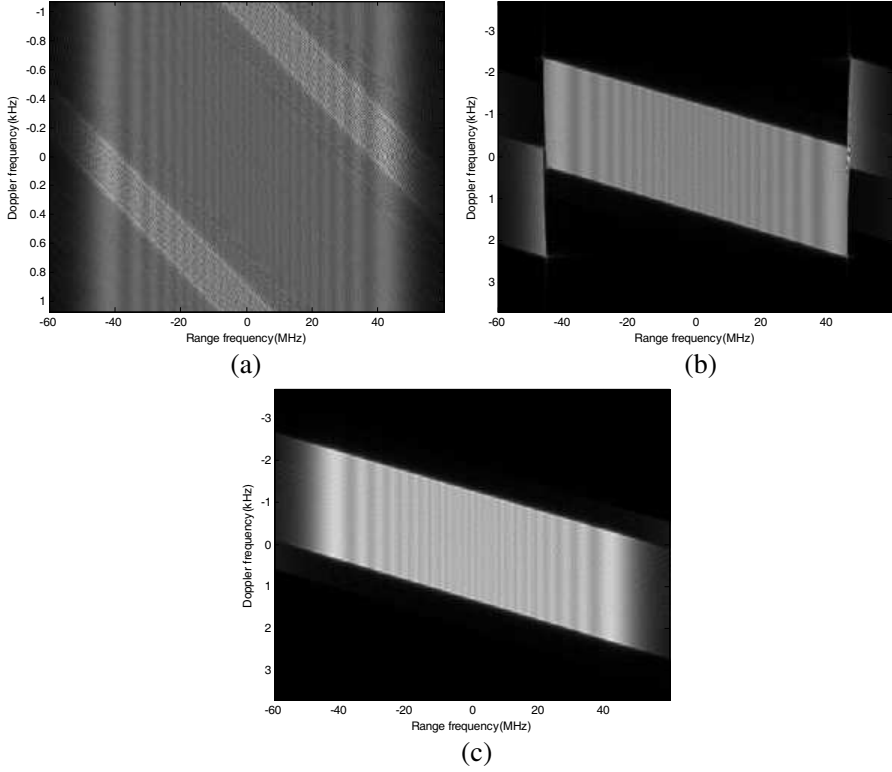
**Figure 5.** (a) 2-D spectrum of original signal. (b) Spectrum processed by traditional TSPA. (c) Spectrum processed by proposed approach.

The residual phase includes the residual range cell migration (RCM), range-azimuth coupling, and azimuth modulation

The second step of conventional RMA is differential focusing. This step is implemented by conventional Stolt mapping, which replaces the square root factor with the shifted and scaled range frequency variable as below [1]:

$$f'_\tau = \sqrt{(f_c + f_\tau)^2 - \frac{c^2 f_a^2}{4v^2}} - f_c \tag{25}$$

However, conventional Stolt mapping is ineffective at the presence of high-squint angle. The modified Stolt mapping is applied instead of conventional Stolt mapping in this paper. It can be written as:

$$f''_\tau = \sqrt{(f_c + f_\tau)^2 - \frac{c^2 f_a^2}{4v^2}} - \sqrt{f_c^2 - \frac{c^2 f_a^2}{4v^2}} \tag{26}$$

After the modified Stolt mapping, the residual phase term becomes

$$\theta_{RES}\left(f_\tau'', f_a\right) = -j\frac{4\pi\left(r - r_{ref0}\right)}{c}\left(\sqrt{f_c^2 - \frac{c^2 f_a^2}{4v^2}} + f_\tau''\right) \qquad (27)$$

Obviously, the modified Stolt mapping separates the residual azimuth compression from the residual RCM correction (RCMC) and the residual range-azimuth coupling compensation, while all of them are implemented in the conventional Stolt mapping. Because residual azimuth compression is range dependent, it should be carried out in range-Doppler domain. According to (27), the residual azimuth compression can be carried out in the range-Doppler domain via the following transfer function:

$$H_4(r, f_a) = \exp\left\{j\frac{4\pi(r - r_{ref0})}{c}\sqrt{f_c^2 - \frac{c^2 f_a^2}{4v^2}} + j2\pi f_a\frac{r_c\sin\left(\theta_0\right)}{v}\right\} \tag{28}$$

The first exponential term in (28) is for the residual azimuth compression, and the second exponential term is applied to correct the time shift in azimuth direction caused by the squint angle [13, 19]. It is deserved to note that the range frequency and range time sampling intervals should be updated according to (26).

## 4. SIMULATION EXPERIMENTS

In order to demonstrate the effectiveness of the proposed approach, a simulation of squinted spotlight SAR is carried out in this section. The specific simulation parameters are listed in Table 2.
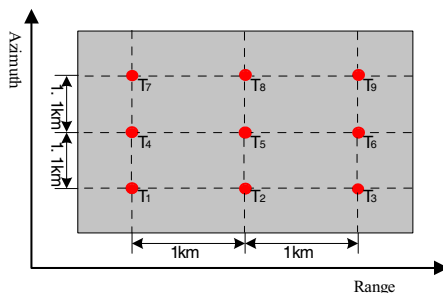


**Figure 6.** The illuminated spot scene.

**Table 2.** System parameters.

| Parameters | Value |
|---|---|
| Carrier frequency | 9.6 GHz |
| Antenna length | 6 m |
| System PRF | 2332 Hz |
| Pulse duration | 1 μs |
| Pulse bandwidth | 200 MHz |
| Sampling frequency | 240 MHz |
| Effective velocity (middle) | 7000 m/s |
| Slant range of imaged center | 600 km |
| Squint angle | 20° |

**Table 3.** Imaging parameters on the simulated point targets.

| Targets | Azimuth | | | Range | | |
|---|---|---|---|---|---|---|
| | Res. | PSLR | ISLR | Res. | PSLR | ISLR |
| | (m) | (dB) | (dB) | (m) | (dB) | (dB) |
| Theoretical Value | 1.03 | −13.26 | −9.80 | 0.89 | −13.26 | −9.80 |
| $T_1$ | 1.03 | −13.31 | −9.94 | 0.90 | −13.27 | −10.05 |
| $T_5$ | 1.03 | −13.28 | −9.94 | 0.90 | −13.27 | −10.05 |
| $T_9$ | 1.03 | −13.25 | −9.89 | 0.90 | −13.18 | −10.00 |

Nine point targets are located in the illuminated spot scene as shown in Fig. 6. Corresponding SAR images processed by different algorithms are shown in Fig. 7. No weighting function has been used in the simulation. Fig. 7(a) shows the result obtained by traditional TSPA. Due to the impacts of the squint angle, "ghost targets" (marked by circles, while real targets are marked by squares) can be observed. The focused SAR image obtained by the presented approach in this paper is shown in Fig. 7(b). It can be seen that all targets are well focused without any "ghost targets".

To further analyze the quality of the focused image obtained by the proposed approach, a quantitative analysis has been carried out on three different point targets $T_1$, $T_5$ and $T_9$, and their contour plots and range/azimuth slices are shown in Fig. 8. Some parameters of targets including the resolution (Res.), peak sidelobe ratio (PSLR) and
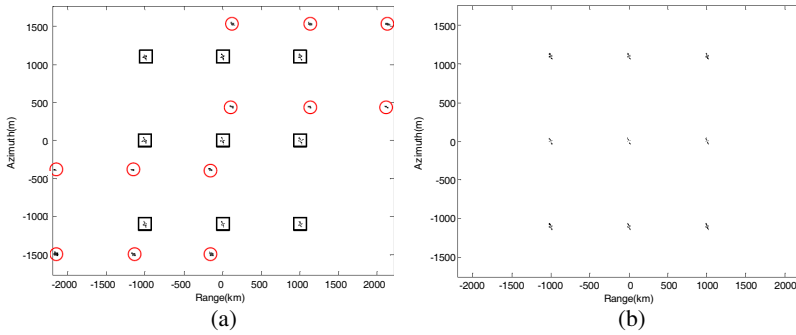
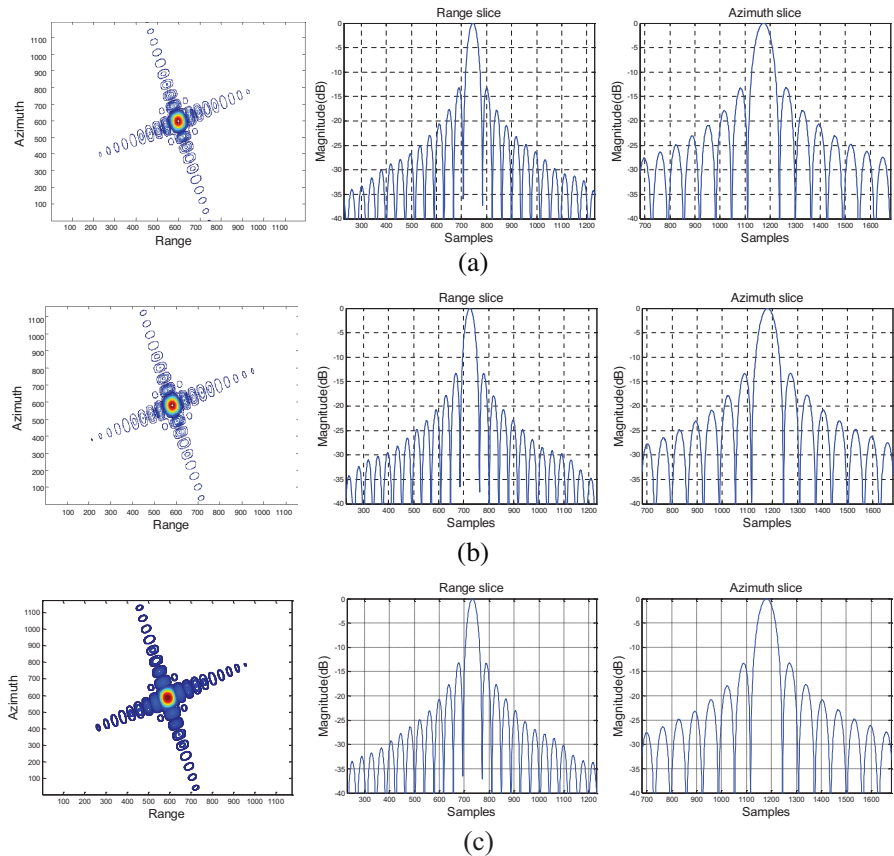**Figure 7.** Processing results with different algorithms. (a) Traditional TSPA. (b) Presented approach.



**Figure 8.** Contour plots and range and azimuth slices of point targets at different positions. (a) Target $T_1$. (b) Target $T_5$. (c) Target $T_9$.

integrated sidelobe ratio (ISLR) are computed and listed in Table 3, which can provide a quantitative evaluation on the targets focused quality [1]. It can be seen that parameters of targets agree with the theoretical values in Table 3. Both the contour plots and quality analysis results validate the effectiveness of the proposed approach.

## 5. CONCLUSION

Owing to the squint angle and azimuth beam steering, the azimuth spectrum folding phenomena in the squinted spotlight mode will seriously affect the focused result. A novel approach for the squinted spotlight SAR focusing is proposed in this paper. This approach employs an improved azimuth preprocessing step, which can effectively remove the impacts of the squint angle and azimuth beam steering on the azimuth spectrum. After azimuth preprocessing, the correct azimuth spectrum is to be obtained. Precise focusing of the squinted spotlight SAR data is achieved by the modified RMA, in which modified Stolt mapping is applied. Furthermore, the proposed approach follows the same fundamental structure of traditional TSPA and keeps its advantage of combining the efficiency of SPECAN algorithm with the precision of stripmap mode focusing techniques. Experiment results carried out on simulated data prove that the proposed approach is effective for the squint spotlight SAR data.

## ACKNOWLEDGMENT

## REFERENCES

1. Cumming, I. G. and F. H. Wong, *Digital Processing of Synthetic Aperture Radar Data: Algorithms and Implementation*, Artech House, Norwood, MA, 2005.
2. Chan, Y. K. and V. C. Koo, "An introduction to Synthetic Aperture Radar (SAR)," *Progress In Electromagnetics Research B*, Vol. 2, 27–60, 2008.
3. Carrara, W. G., R. S. Goodman, and R. M. Majewski, *Spotlight*

*Synthetic Aperture Radar—Signal Processing and Algorithms*, Artech House, Boston, MA, 1995.

4. Sun, J., S. Mao, G. Wang, and W. Hong, "Polar format algorithm for spotlight bistatic SAR with arbitrary geometry configuration," *Progress In Electromagnetics Research*, Vol. 103, 323–338, 2010.

5. Cantalloube, H. and P. Dubois-Fernandez, "Airborne X-band SAR imaging with 10 cm resolution: Technical challenge and preliminary results," *IEE Proc Radar Sonar Navig.*, Vol. 152, 163–176, 2006.

6. Mittermayer, J., B. Schättler, and M. Younis, "TerraSAR-X commissioning phase execution summary," *IEEE Trans. Geosci. Remote Sens.*, Vol. 48, No. 2, 649–659, 2010.

7. Lanari, R., P. Franceschetti, M. Tesauro, and E. Sansosti, "Spotlight SAR image generation based on strip mode focusing techniques," *Proc. IGARSS*, 1761–1763, Hamburg, Germany, 1999.

8. Lanari, R., M. Tesauro, E. Sansosti, and G. Fornaro, "Spotlight SAR data focusing based on a two-step processing approach," *IEEE Trans. Geosci. Remote Sens.*, Vol. 39, No. 9, 1993–2004, 2001.

9. Ren, X.-Z., Y. Qin, and L. H. Qiao, "Interferometric properties and processing for spaceborne spotlight SAR," *Progress In Electromagnetics Research B*, Vol. 36, 267–281, 2012.

10. Xu, W., P. P. Huang, and Y.-K. Deng, "Multi-channel SPCMB-TOPS SAR for high-resolution wide-swath imaging," *Progress In Electromagnetics Research*, Vol. 116, 533–551, 2011.

11. Prati, C., A. M. Guarnieri, and F. Rocca, "Spot mode SAR focusing with the omega-k technique" in *Proc. IGARSS*, 631–634, Helsinki, Finland, 1991.

12. Mittermayer, J., A. Moreira, and O. Loffeld, "Spotlight SAR data processing using the frequency scaling algorithm," *IEEE Trans. Geosci. Remote Sens.*, Vol. 37, No. 5, 2198–2214, 1999.

13. Davidson, G. W., I. G. Cumming, and M. R. Ito, "A chirp scaling approach for processing squint mode SAR data," *IEEE Trans. Aerosp. Electron. Syst.*, Vol. 32, No. 1, 121–133, 1996.

14. Moreira, A. and Y. Huan, "Airborne SAR processing of highly squinted data using a chirp scaling approach with integrated motion compensation," *IEEE Trans. Geosci. Remote Sens.*, Vol. 32, No. 5, 1029–1040, 1994.

15. Davidson, G. W. and I. G. Cumming, "Signal properties of spaceborne squint mode SAR," *IEEE Trans. Geosci. Remote*

*Sens.*, Vol. 35, No. 3, 611–617, 1997.

16. An, D. X., X. T. Huang, T. Jin, and Z. M. Zhou, "Extended two-step focusing approach for squinted spotlight SAR imaging," *IEEE Trans. Geosci. Remote Sens.*, Vol. 50, No. 7, 2889–2900, 2012.

17. An, D. X., Z. M. Zhou, X. T. Huang, and T. Jin, "A novel imaging approach for high resolution squinted spotlight SAR based on the deramping-based technique and azimuth NLCS principle," *Progress In Electromagnetics Research*, Vol. 123, 485–508, 2012.

18. Reigber, A., E. Alivizatos, A. Potsis, and A. Moreira, "Extended wavenumber-domain synthetic aperture radar focusing with integrated motion compensation," *IEE Proc Radar Sonar Navig.*, Vol. 153, No. 3, 301–310, 2006.

19. Guo, D., H. Xu, and J. Li, "Extended wavenumber domain algorithm for highly squinted sliding spotlight SAR data processing," *Progress In Electromagnetics Research*, Vol. 114, 17–32, 2011.

20. Wong, F. H. and T. S. Yeo, "New application of nonlinear chirp scaling in SAR data processing," *IEEE Trans. Geosci. Remote Sens.*, Vol. 39, No. 5, 946–953, 2001.

21. Kim, K. T., S. H. Park, and J. I. Park, "Motion compensation for squint mode spotlight SAR imaging using efficient 2D interpolation," *Progress In Electromagnetics Research*, Vol. 128, 503–518, 2012.